Journal of Transport Geography 130 (2026) 104470

Contents lists available at ScienceDirect

Journal of Transport Geography

journal homepage: www.elsevier.com/locate/jtrangeo

Uncovering the sensing power of shared bikes for urban feature monitoring

Wen Ji [a,c,1], Ke Han [b,1], Qi Hao [c], Qian Ge [b], Ying Long [c,d,*]

[a] School of Transportation and Logistics, Southwest Jiaotong University, Chengdu, Sichuan 611756, China
[b] School of Economics and Management, Southwest Jiaotong University, Chengdu, Sichuan 610031, China
[c] School of Architecture, Tsinghua University, Beijing, China
[d] Hang Lung Center for Real Estate, Key Laboratory of Eco Planning & Green Building, Ministry of Education, Tsinghua University, Beijing, China

ARTICLE INFO

Keywords:
Urban sensing
Bike-sharing system
Sensor deployment
Spatial–temporal coverage
Bike rebalancing

ABSTRACT

The development of smart cities demands cost-effective sensing solutions for community-level urban diagnostics. Bike-sharing systems could serve as an ideal mobile sensing platform due to their unparalleled ability to access fine-grained urban capillaries at street level, combining both physical and direct observability of built structures. This study represents the first systematic effort to explore the potential of shared bikes as a novel mobile sensing platform. Moving beyond the limitations of existing research, which predominantly focuses on post-collection data analysis while overlooking data acquisition optimization, we propose an integrated simulation–optimization framework. This framework simultaneously minimizes fleet size, optimizes daily rebalancing operations, and generates complete monthly trajectory data. Furthermore, we develop a day-to-day optimization model for deploying sensor-equipped bikes, which co-determines initial allocation and daily dispatch strategies under budget constraints. A simulation-based case study in Manhattan demonstrates that the proposed strategy improves the sensing reward by 4%–8% compared to random deployment. At a monthly interval, only 100 shared bikes (approximately 1% of the fleet) are needed to cover 81% of road segments. Transferability analyses conducted in San Francisco and Longquanyi District, Chengdu, reveal that sensing performance is largely influenced by local cycling patterns. This research offers a conceptually innovative, low-cost, and scalable sensing solution for fine-grained urban management.

1. Introduction

The rapid urbanization of cities has intensified demand for innovative sensing solutions to monitor complex urban dynamics efficiently (Du et al., 2019). Drive-by sensing (DS), which leverages sensor-equipped vehicles for spatial–temporal data collection, has gained prominence due to its cost-effectiveness and extensive coverage potential (Birenboim et al., 2021; Ji et al., 2023a; Ma et al., 2014; Anjomshoaa et al., 2018). The selection of appropriate sensing platforms depends critically on specific monitoring requirements. For air quality (Hasenfratz et al., 2015; Nagendra Shiva et al., 2019) and urban heat island phenomena (Fekih et al., 2021), high-frequency sampling at high spatial resolutions (typically 1 km grids) is essential. Taxis (O'Keeffe et al., 2019; Chen et al., 2020; Hou et al., 2025b) and buses (Ji et al., 2023b; Ariss et al., 2024; Huang et al., 2024), with their expansive operational ranges and continuous service patterns, are well-suited for such grid-based monitoring. In contrast, dedicated sensing vehicles remain confined to targeted small-scale inspections due to their substantial deployment costs (Messier et al., 2018; Glock and Meyer, 2020).

Urban feature monitoring[2] requires high spatial resolution but relatively low temporal frequency. As illustrated in Fig. 1, applications including vacancy storefront detection (Li and Long, 2024), abandoned building identification (Li et al., 2023), road occupation detection (Ma et al., 2025), road surface quality monitoring (Li et al., 2019), environment hygiene monitoring (Grubesic et al., 2018) and building facade quality monitoring (Wallace and Schalliol, 2015) necessitate street-level spatial detail with daily, weekly, or monthly sampling sufficiency. Conventional platforms face fundamental limitations: taxis and buses, constrained by restricted maneuverability, are largely confined to arterial roads and thus unable to penetrate finer urban fabrics, while dedicated vehicles remain economically prohibitive for systematic city-scale deployment.

The limitations of conventional sensing platforms hinder comprehensive urban feature monitoring, creating a need for an alternative

* Correspondence to: Room 501, New Architecture Building, Tsinghua University, Haidian District, Beijing, 100084, China.
E-mail address: ylong@tsinghua.edu.cn (Y. Long).
[1] These authors contributed equally to this work.
[2] We define "urban features" as physical, functional, and perceptual attributes observable at street-view level.

https://doi.org/10.1016/j.jtrangeo.2025.104470
Received 15 April 2025; Received in revised form 21 October 2025; Accepted 24 October 2025

Fig. 1. Representative urban features monitoring scenarios.

that offers both the mobility to access fine-grained urban spaces and the scalability for cost-effective city-wide deployment. Within this context, the bike emerges as a highly suitable mobile sensing platform, owing to its intrinsic agility and ease of deployment. The use of sensor-equipped bikes is well documented in transportation studies, where sensors such as GPS, cameras, and accelerometers are commonly used to gather data related to the biking experience, encompassing riding behavior, safety metrics, and pavement conditions (Gadsby and Watkins, 2020).

This study extends the sensor-equipped bike paradigm by examining bike-sharing systems as a scalable and systematic approach to urban feature monitoring. Unlike earlier work focused on the biking experience, we reconceptualize the bike as a versatile data collection tool capable of capturing diverse urban attributes. Specifically, bike-sharing systems offer three distinctive advantages as an urban sensing platform: (1) their ability to penetrate confined and complex urban areas such as alleyways, parks, and mixed-use zones, which are often unreachable by motorized vehicles; (2) their lower travel speed, which supports high-resolution street-level imaging and enables the capture of architectural and infrastructural details typically missed by faster-moving platforms; and (3) the typical routing of bikes along building facades, which ensures clear and unobstructed views of structural surfaces. From a commercial perspective, these capabilities enable the development of "Sensing as a Service" models, creating additional revenue streams for operators through the monetization of urban intelligence related to infrastructure conditions, commercial activity, and environmental factors (Shen et al., 2022).

Existing research leveraging bike-sharing systems for urban sensing remains preliminary. While studies such as Wu et al. (2020) and Voinea et al. (2020) demonstrate the feasibility of air quality monitoring using sensor-equipped bikes, their focus is primarily confined to post-collection data analysis. These works have not systematically addressed the optimization of data acquisition processes, particularly in terms of sensor deployment strategies or operational scheduling. This oversight constitutes a critical research gap that limits the full realization of bike-sharing systems as urban sensing platforms. To address this gap, we aim to maximize the sensing power of shared bike fleets. Specifically, our contributions are as follows:

(1) We develop an integrated simulation–optimization framework for shared bike systems that jointly determines the minimum fleet size, optimizes daily rebalancing operations, and generates complete monthly bike trajectories using real trip data.
(2) We propose a day-to-day optimization framework for sensor-equipped bike deployment, co-optimizing initial allocation and daily repositioning while quantifying sensing power under varying budgets.
(3) We validate the sensor optimization strategy through a Manhattan case study, demonstrating its capability to enhance sensing reward by 4%–8% compared to random deployment. Subsequent transferability studies in San Francisco and Chengdu's Longquanyi District reveal that the sensing power of shared bike fleets is primarily governed by local bike usage patterns.

The remainder of this paper is organized as follows: Section 2 provides a review of relevant literature. Section 3 outlines the research framework, methodology, and data employed in this study. The results and corresponding discussions are presented in Section 4, and finally, the conclusions are drawn in Section 5.

2. Related work

2.1. Drive-by sensing with different vehicles

In recent years, diverse vehicle types have been utilized for urban sensing, with their spatial–temporal sampling quality largely influenced by their mobility patterns (Anjomshoaa et al., 2018). For instance, O'Keeffe et al. (2019) quantified the sensing power of taxi fleets by combining a stochastic process with a ball-in-bin model, revealing that hot spot areas are frequently covered while remote regions are often overlooked. Similarly, Ariss et al. (2024) and Ji et al. (2023b) investigated the deployment of sensors in bus fleets, showing that only 1–2 sensors per route are sufficient to ensure hourly coverage of all segments, albeit within the geographic limitations of the bus network. On the other hand, Ji et al. (2025) proposed an adaptive large neighborhood search algorithm to dynamically schedule dedicated vehicles for volatile organic compound (VOC) monitoring, offering high adaptability but at significant deployment and operational costs. Han et al. (2024) addresses the problem of how to optimally allocate sensors across a mixed fleet of taxis, buses, and dedicated vehicles, as well as how to select bus routes and schedule dedicated vehicles, in order to provide optimal spatial–temporal coverage for the monitoring area. Table 1 summarizes these insights, highlighting key

Table 1
Comparative analysis of vehicular sensing platforms.

Vehicle Type	Coverage characteristics	Sensing limitations
Taxis	High-frequency coverage in hotspots	Limited penetration into intra-block areas; blind spots in remote regions
Buses	Periodic coverage along fixed routes	Limited to bus network
Dedicated vehicles	Customizable full-area coverage	Prohibitive operational costs
Shared bikes	**Penetrates urban capillaries: alleyways, parks, vehicle-inaccessible blocks**	**Weather dependent**

coverage characteristics and fundamental constraints across vehicular sensing platforms.

For urban feature monitoring requiring fine spatial resolution at street level as illustrated in Fig. 1, shared bikes provide unique advantages through their ability to penetrate urban capillaries like alleyways, parks, and mixed use blocks, capture high resolution imagery during slower movement, and conduct proximity sensing along building facades. This capability combination enables acquisition of micro scale physical, functional, and perceptual attributes unattainable by conventional platforms.

2.2. Sensor deployment and dispatch problems in drive-by sensing

Research on sensor deployment and dispatch for DS mainly focuses on taxis, buses and dedicated vehicles, employing two distinct paradigms: strategic sensor installation and operational control. For taxis, some studies aim to optimize vehicle subset selection. For instance, Zhao et al. (2014) design a greedy heuristic algorithm to select the minimum number of taxis required to meet specified monitoring requirements. Zhang et al. (2018) develop a multi-objective genetic algorithm to identify an optimal subset of taxis that jointly optimizes the overall coverage of all vehicles and the reliability of individual sensing tasks. Hou et al. (2025a) propose a vehicle selection algorithm for advancing vehicular sensing power with higher regular coverage on both future hotspots and non-hotspots. While others enhance sensing through operational strategies like vehicle–passenger matching (Meng and Han, 2023; Chen et al., 2020) and incentivizing routing for both occupied (Asprone et al., 2021) and unoccupied vehicles (Guo and Qian, 2024). For buses, some studies aim to select an optimal subset of bus routes or vehicles for sensor installation to maximize sensing rewards. For instance, Kaivonen and Ngai (2020) employ a route coverage image analysis algorithm to determine the best combination of bus routes for maximizing spatial coverage. Gao et al. (2016) design a greedy heuristic algorithm to select a subset of buses that maximizes the sensing reward. Agarwal et al. (2020) introduce an approximate algorithm for selecting a subset of vehicles from a mixed fleet of buses and taxis to maximize sensing reward. While others focus on the joint optimization of timetable coordination and vehicle scheduling to maximize sensing rewards (Ji et al., 2023b; Dai and Han, 2023). For dedicated vehicles, specific route planning algorithms are typically developed to achieve maximum sensing efficiency (Ji et al., 2025).

However, bike-sharing system poses unique sensing challenges: user-driven trajectory uncertainty, dynamic inventory constraints, and distinct operational characteristics. Our response pioneers (1) a probabilistic coverage model (Section 3.4.2) establishing binomial stand-to-road correlations, eliminating trajectory dependency; and (2) an integrated MILP framework (Section 3.4.3) co-optimizing sensor allocation and daily dispatch.

3. Material and methods

3.1. Overview

This study aims to uncover the sensing power of bike-sharing systems in urban feature monitoring. The methodological framework is shown in Fig. 2. Table 2 lists key parameters and variables used in this paper.

(1) **Data processing**: The input includes bike-sharing trip data and OpenStreetMap (OSM) road network data. This part first describes the extraction of bike-specific network from the OSM network (Section 3.2.1), followed by the cleaning of trip order data for subsequent trajectory simulation (Section 3.2.2).
(2) **Simulation of bike operation**: This part introduces a simulation method based on bike-sharing trip data and stand information to estimate the total number of bikes and generate individual bike trajectories. Further details can be found in Section 3.3.
(3) **Sensor deployment and dispatch**: Building on the proposed sensing power quantification metric (Section 3.4.1) and bike-road binary distribution relationship (Section 3.4.2), we develop a day-to-day optimization framework for sensor allocation and daily re-dispatch schedules under sensor budget constraint, maximizing the sensing reward. Further details can be found in Section 3.4.3.

3.2. Data processing

3.2.1. Road network processing

The Manhattan road network data are retrieved from the OpenStreetMap website.[3] To generate a bike-specific network that accurately reflects paths usable by shared bikes, a series of detailed preprocessing steps are applied:

- **Filtering by road type:** The raw OSM data is filtered to remove road types explicitly unsuitable for bicycle traffic. Specifically, all roads tagged as "motorway", "motorway link", "trunk", and "trunk link" are excluded. This ensures only roads legally and practically accessible to bicycles are retained.
- **Multi-Lane merging:** For roads comprising multiple parallel lanes designated for bicycle traffic (e.g., separate lanes for each direction or adjacent bike paths), these lanes are merged into a single representative path per physical road segment. This prevents overcounting or redundant representation of the same physical roadway in the network.
- **Residential area simplification:** Within areas tagged as "residential" or "living street", particularly focusing on internal footway' paths within housing complexes, a simplification is performed. Only key internal connectors providing essential through-access (e.g., primary lanes or streets traversing a block) are retained. Minor internal footpaths serving only localized access are removed.
- **Park/Greenspace simplification:** For large green spaces like central park and similar areas with dense internal path networks, the network is simplified by retaining only the primary internal circulation routes while removing minor trails that would not typically serve as main bicycle thoroughfares.

[3] OpenStreetMap: https://www.openstreetmap.org.

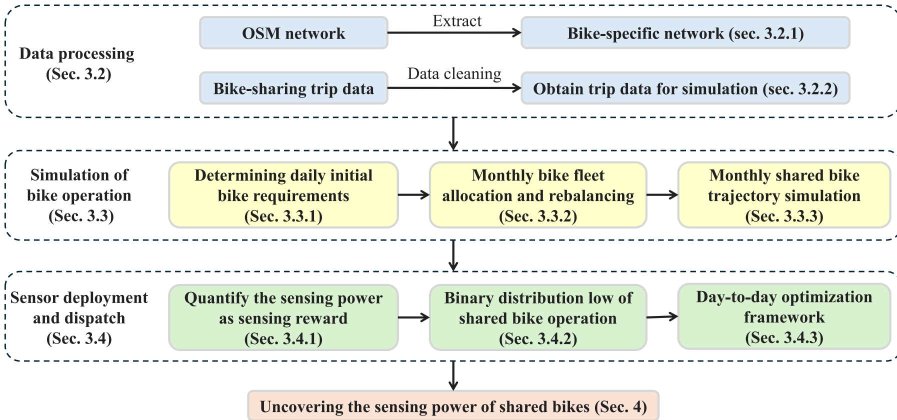

Fig. 2. Methodological framework.

Table 2
Notations and symbols.

Sets	
$\mathcal{D}$	Set of days within a month;
$\mathcal{R}_d$	Set of bike trips on day d;
$\mathcal{S}$	Set of bike stands;
$\mathcal{I}$	Set of shared bikes;
$\mathcal{T}$	Set of monthly bike trajectories;
$\mathcal{C}$	Set of time periods;
Parameters and constants	
t_0	Start time of daily operations;
T	End time of daily operations;
$b_{s,d}$	Minimum initial bike number required for stand s on day d;
N_b	Total bike fleet size;
$\delta_{s,d}$	Net change of bikes at stand s by the end of day d;
$\mathrm{TD}(i,j)$	Shortest travel distance between stand i and stand j, where $i, j \in \mathcal{S}$;
$N_{s,e}$	Number of times the road segment e has been covered by sensor-equipped bikes at stand s;
N_k	Total number of sensors;
N_C	Total number of time periods;
$p_{s,e}$	Probability that a bike originating from stand s intersects road segment e during a single day;
N_e	Number of sensor-equipped bikes covering road segment e during time period;
l_e	Length of road segment e;
Auxiliary variables	
$\gamma_{s,d}$	Net change of sensor-equipped bikes at stand s by the end of day d;
y_e	Binary variable that equals 1 if the expected coverage of road segment e during time period exceed K times;
Decision variables	
$z_{s,d}$	Actual number of bikes deployed at stand s at the beginning of day d;
$x_{s,d}$	Number of sensor-equipped bikes at station s at the beginning of day d;
$x_{i,j,d}$	Quantity of bikes relocated from stand i to stand j during the nightly rebalancing operation after day d;
$y_{i,j,d}$	Quantity of sensor-equipped bikes relocated from stand i to stand j during the nightly rebalancing operation after day d;

This comprehensive preprocessing results in a refined bicycle-accessible network that more realistically represents the routes commonly utilized by shared bike users in Manhattan, as shown in Fig. 3 (Left).

3.2.2. *Bike-sharing trip data processing*

Bike-sharing trip data for Manhattan covering the entire month of March 2024 are obtained from the official website of the Citi Bike operator.[4] This data provides the origin and destination station locations, as well as the start time and end time for each trip. However, detailed trajectory information is not included. The trip data undergoes the following preprocessing steps:

- **Step 1:** The bike stands are mapped to the nearest nodes on the road network based on their coordinates. This process identifies 647 unique bike stands within the Manhattan road network, as shown in Fig. 3 (Right).
- **Step 2:** For each trip, the actual travel duration is calculated directly from the provided start and end times in the trip data. Simultaneously, the shortest path distance between the origin and destination stations is computed using the road network adjacency matrix. The average travel speed for each trip is then determined by dividing the shortest path distance by the actual travel duration. This derived speed value is finally used to dynamically reconstruct the trajectory along the computed shortest path.

[4] NYC (Citi): https://www.citibikenyc.com/system-data.

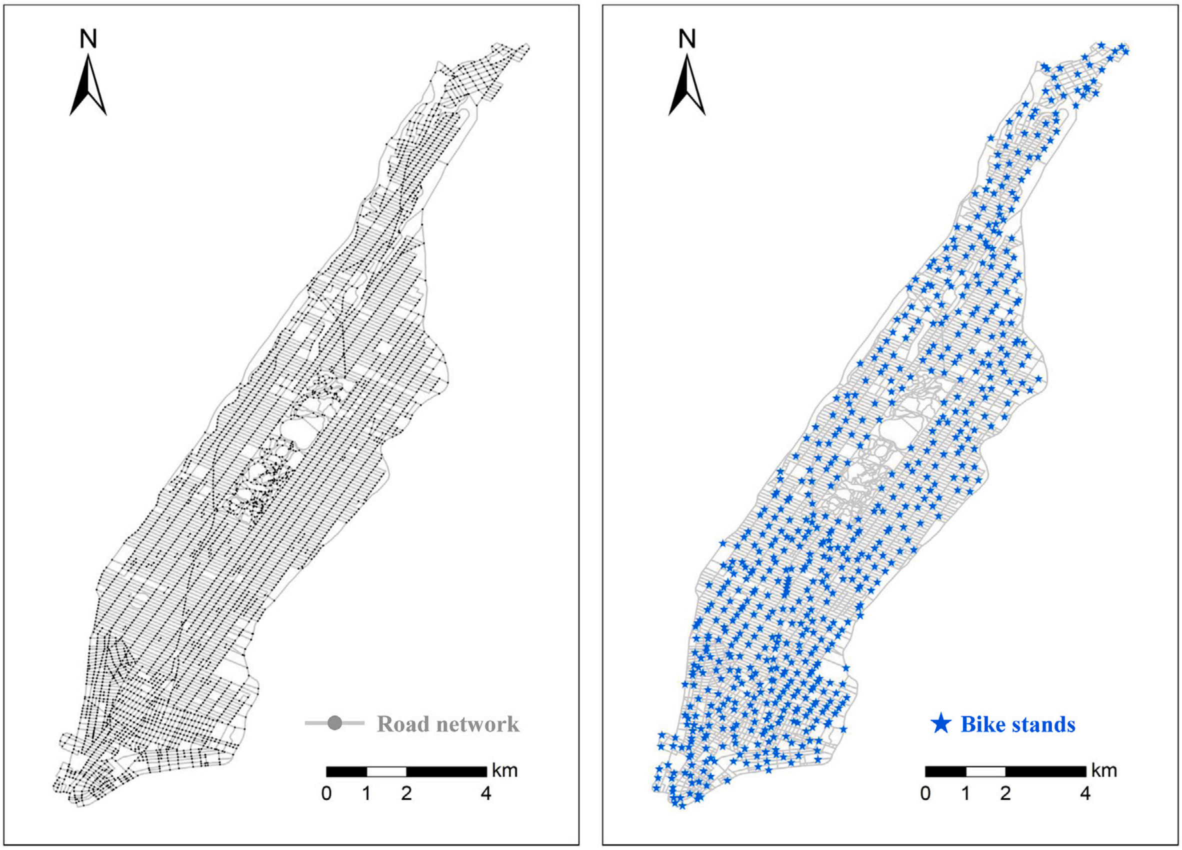

Fig. 3. Left: Road network of Manhattan, New York City, which consists of 3787 nodes and 6833 road segments. Right: Locations of 647 bike-sharing stands in Manhattan.

- **Step 3:** Trips are filtered to include only if both their start and end times strictly fall within the 6:00 AM to 8:00 PM, as the demand for data collection during nighttime hours is minimal.
- **Step 4:** To mitigate the influence of anomalous trips that may represent data errors or non-typical cycling behaviors, we apply a distribution-based filtering approach. Specifically, trips falling within the top and bottom 1% of the derived average speed distribution are excluded. This truncation method effectively removes extreme outliers. The resulting speed distribution of the filtered trips is visualized in the histogram presented in Fig. 4.

Following the data processing, 82% of the original trip records are retained. Fig. 5 visualizes the daily order volume during the month of March 2024.

3.3. Simulation of shared bike operations based on trip data

This section presents a methodology for simulating shared bike trajectories over a one-month period. The approach consists of three components: (1) determining daily initial bike requirements, (2) optimizing monthly fleet allocation and rebalancing, and (3) simulating complete bike trajectories.

3.3.1. Daily initial bike requirements

For each day $d \in \{1, 2, \dots, |\mathcal{D}|\}$ in the monthly period, we compute the minimum initial bike number $b_{s,d}$ required for stand $s \in \mathcal{S}$ on day d to satisfy all trip demands, similar to Wu et al. (2024). In this study, we focus exclusively on trips occurring between 6:00 AM and 8:00 PM daily, thus defining $t_0 = 6:00$ AM as the start of daily operations and $T = 8:00$ PM as the end of daily operations. The computation processes daily trip data $\mathcal{R}_d$ through Algorithm 1, which tracks stand occupancy dynamics throughout $[t_0, T]$. The core calculation is:

$$b_{s,d} = \max_{t \in [t_0, T]} \left(-\Delta^t_{s,d} \right)^+ \tag{3.1}$$

where $\Delta^t_{s,d}$ is the cumulative net bike deficit from t_0 to t at stand s on day d, computed as:

$$\Delta^t_{s,d} = \sum_{\tau = t_0}^{t} \left(0 + n^s_{arr,t} - n^s_{dep,t} \right) \tag{3.2}$$

This ensures sufficient bikes to cover the deepest deficit observed during operations. After simulation, we compute the daily total shared bike requirement $b_d = \sum_{s \in S} b_{s,d}$ for each day in the monthly period. These daily requirements are visualized in Fig. 6.

The total bike fleet size N_b for this study is determined by the peak daily requirement observed during the month, ensuring sufficient bikes are available even on the highest-demand day. This is formalized as:

$$N_b = \max_{d \in D} b_d = 9581 \tag{3.3}$$

3.3.2. Shared bike fleet rebalancing optimization

To maintain operational continuity across one month, we formulate an integer programming model for nightly bike redistribution. This addresses the mismatch between end-of-day bike distribution and next-day requirements.

Based on the results derived in Section 3.3.1, we have established both the total shared bike fleet size N_b for Manhattan and the minimum required number of bikes $b_{s,d}$ at each stand s at the start of day d. Furthermore, leveraging trip data, we compute $\delta_{s,d}$, the net change in bike count at stand s by the end of day d, where positive values indicate

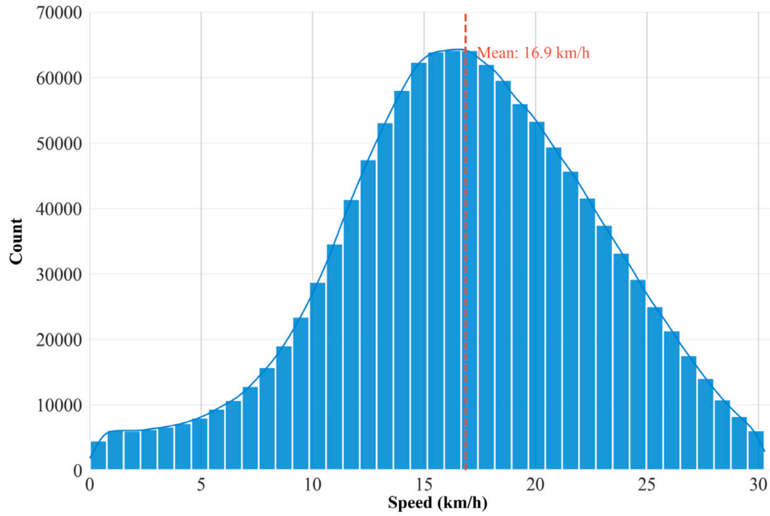

Fig. 4. Histogram of bicycle speeds in Manhattan.

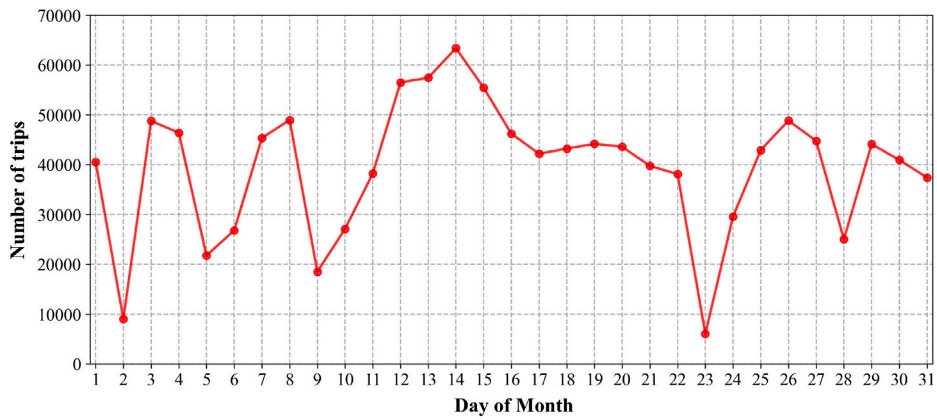

Fig. 5. Daily order volume after trip data processing (March 2024).

Algorithm 1 Compute daily initial bike requirements

Input Daily shared bike trips $\mathcal{R}_d$, Bike stands $\mathcal{S}$, start time t_0, end time T;

For each $d \in \mathcal{D}$:
  For each $s \in \mathcal{S}$:
    $\Delta^t_{s,d} \leftarrow 0$ (cumulative net deficit),
    $\Delta^{\min}_{s,d} \leftarrow 0$ (min cumulative deficit),
    $t = t_0$,
    While $t \leq T$:
      Count the number of arriving trips at stand s at time t: $n^s_{arr,t}$
      Count the number of departing trips from stand s at time t: $n^s_{dep,t}$
      Update cumulative deficit: $\Delta^t_{s,d} \leftarrow \Delta^t_{s,d} + n^s_{arr,t} - n^s_{dep,t}$
      Update min deficit:$\Delta^{\min}_{s,d} \leftarrow \min(\Delta^{\min}_{s,d}, \Delta^t_{s,d})$;
      Update time: $t = t + 1$;
    End While
    Initial number of bikes at stand s: $b_{s,d} \leftarrow \max(0, -\Delta^{\min}_{s,d})$;
  End For
  The total number of bikes required for day d: $b_d = \sum_{s \in \mathcal{S}} b_{s,d}$;
End For

Output $b_{s,d}$, $\forall s \in \mathcal{S}, d \in \mathcal{D}$ and total number of bikes b_d for day d, $\forall d \in \mathcal{D}$.

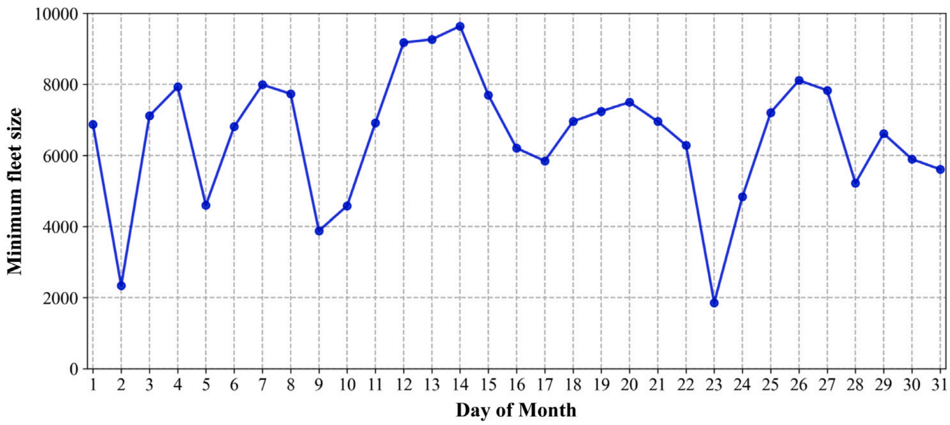

Fig. 6. Daily Minimum shared bike fleet size requirement in March 2024.

net gains and negative values represent net losses. To resolve the bike rebalancing problem, we introduce decision variable $z_{s,d}$ to represent the actual number of bikes deployed at stand s at the beginning of day d, along with variable $x_{i,j,d}$ to denote the quantity of bikes relocated from stand i to stand j during the nightly rebalancing operation after day d. The optimization model of shared bike fleet rebalancing problem is formally presented below:

$$\min \sum_{d\in\mathcal{D}}\sum_{i\in\mathcal{S}}\sum_{j\in\mathcal{S}} x_{i,j,d} TD(i,j) \tag{3.4}$$

such that

$$z_{s,d+1} = z_{s,d} + \delta_{s,d} + \sum_{i\in\mathcal{S}} x_{i,s,d} - \sum_{j\in\mathcal{S}} x_{s,j,d} \quad \forall s \in \mathcal{S}, \forall d \in \{1,2,\dots,|\mathcal{D}|-1\} \tag{3.5}$$

$$z_{s,d} + \delta_{s,d} \geq \sum_{j\in\mathcal{S}} x_{s,j,d} \quad \forall s \in \mathcal{S}, \forall d \in \{1,2,\dots,|\mathcal{D}|-1\} \tag{3.6}$$

$$\sum_{s\in\mathcal{S}} z_{s,d} = N_b \quad \forall d \in \mathcal{D} \tag{3.7}$$

$$z_{s,d} \geq b_{s,d} \quad \forall s \in \mathcal{S}, \forall d \in \mathcal{D} \tag{3.8}$$

$$z_{s,d} \in \mathbb{Z}^+ \quad \forall s \in \mathcal{S}, \forall d \in \mathcal{D} \tag{3.9}$$

$$x_{i,j,d} \in \mathbb{Z}^+ \quad \forall i,j \in \mathcal{S}, \forall d \in \mathcal{D} \tag{3.10}$$

The objective function (3.4) minimizes total relocation costs, where $TD(i,j)$ represents the shortest travel distance between stand i and stand j. Constraints (3.5) establishes a deterministic state transition equation that governs the temporal evolution of bike inventory across the station network. Constraint (3.6) makes sure that cannot move out more bikes than actually exist at a station. Constraints (3.7) guarantee the total number of bikes in the entire system always stays the same. Constraints (3.8) guarantee sufficient bikes to meet operational requirements. Constraints (3.9) and (3.10) are the decision variable constraints. The above model can be directly solved by off-the-shelf solvers.

3.3.3. Monthly shared bike trajectory simulation

After the daily initial bike requirements and the shared-bike rebalancing scheme are determined, we obtain a fixed fleet $\mathcal{I}$ of N_b shared bikes and daily start-of-day inventories $z_{s,d}$ for every stand $s \in \mathcal{S}$ and every day $d \in \mathcal{D} = \{1,\dots,31\}$. In addition, the overnight rebalancing plan $x_{i,j,d}$ prescribes the number of bikes to be moved from stand i to stand j after the completion of day d. The objective of the present section is to generate, for every bike $k \in \mathcal{I}$, a complete one-month trajectory that is consistent with these inputs as well as with the trip data $\mathcal{R}_d$ collected on each day.

Algorithm 2 constructs, for a single day d, the complete set of N_b trajectories from the trip list $\mathcal{R}_d$ and the prescribed start-of-day inventory $z_{s,d}$. Initialize prepare an empty trajectory list $\{\tau_i^d\}_{i=1}^{N_b}$ and a state array $\mathcal{Q}$ whose ith entry records the current station, a busy flag, and the release time of trajectory i; the array is initialized so that the first $z_{s,d}$ positions for every stand s point to s and all trajectories are idle. The global clock t is set to the simulation start t_0. Within the main loop (Steps 1–13) the algorithm advances time in unit steps. At each time t it first scans the state array (Steps 2–4) and resets the busy flag to false for any trajectory whose scheduled release time has been reached. Next, it extracts all trips starting at time t into the set $\mathcal{R}'$ (Step 5). For every such trip r, lines 6–11 identify the set $\mathcal{A}$ of currently idle trajectory located at the trip origin o_r, uniformly selects an index i^* from $\mathcal{A}$, appends the tuple $(t, o_r, \text{destination}(r), p_r)$ to trajectory τ_{i^*}, and updates the corresponding entry in $\mathcal{Q}$ to reflect the new stand, the busy status, and the expected completion time. After processing all trips at the current time step the clock is incremented (Step 12), and the loop repeats until the simulation end time T is reached. The algorithm finally returns the multiset $\{\tau_i^d\}_{i=1}^{N_b}$, where each τ_i^d is an ordered list of tuples encoding the complete day-d itinerary.

Algorithm 3 synthesizes complete monthly bike trajectories through sequential daily processing. It begins by establishing day-1 assignments: each bike is initialized to its starting stand according to inventory $z_{s,1}$ and is allocated a random day-1 trajectory from origin-compatible options via non-repetitive sampling (Steps 1–8). For subsequent days (Steps 9–12), overnight rebalancing $x_{i,j,d}$ first relocates bikes between stands, whereupon day-$(d+1)$ trajectories are assigned using identical origin-constrained sampling logic. This process maintains strict inventory consistency while ensuring each daily trajectory fragment is uniquely assigned exactly once per day.

3.4. Deployment and dispatch of sensor-equipped bikes

This section first presents a system level road coverage metric Φ in Section 3.4.1. Section 3.4.2 then uses a binomial hypothesis and trajectory data to quantify the relation between the number of bikes at stands and the coverage of road segments. Building on these findings, Section 3.4.3 formulates a mixed integer linear programming model within the total sensor budget N_k, simultaneously determines the sensor allocation and the nightly re-dispatch schedule to maximize sensing reward Φ.

3.4.1. Quantify the sensing power as sensing reward

We introduce a metric to quantify the sensing power of bike-sharing systems under different monitoring frequencies. The time is divided into distinct monitoring period $\omega \in C$ (e.g., days, weeks, or months). The sensing reward for a road segment is defined based on whether it is covered by at least one sensor-equipped bike within each time period ω. Let $N_{e,\omega}$ represent the number of sensor-equipped bikes covering road segment e during monitoring time period ω. The corresponding sensing

Algorithm 2 Intraday trajectory generation

Input Trips $\mathcal{R}_d$, shortest-path p_r for every $r \in \mathcal{R}_d$, bike stands $\mathcal{S}$, start-of-day inventory $z_{s,d}$ $\forall s \in \mathcal{S}$, fleet size N_b, start time t_0, end time T;
Initialize Create N_b empty trajectories $\{\tau_1^d, \dots, \tau_{N_b}^d\}$; create list $\mathcal{Q}$ of length N_b with entries $(s, \text{false}, 0)$, where the first $z_{s,d}$ entries point to stand s; set $t \leftarrow t_0$;
1: While $t \le T$:
2: For every index $i \in \{1, \dots, N_b\}$ with $\mathcal{Q}[i]$.busy = true and end time $\le t$:
3: Set $\mathcal{Q}[i]$.busy $\leftarrow$ false;
4: End For
5: Let $\mathcal{R}' \leftarrow \{r \in \mathcal{R}_d \mid \text{start time}(r) = t\}$;
6: For each $r \in \mathcal{R}'$:
7: Let $o_r \leftarrow \text{origin}(r)$ and form $\mathcal{A} \leftarrow \{i \mid \mathcal{Q}[i].\text{stand} = o_r \wedge \mathcal{Q}[i].\text{busy} = \text{false}\}$;
8: Draw $i^* \sim \text{Uniform}(\mathcal{A})$;
9: Append $(t, o_r, \text{destination}(r), p_r)$ to $\tau_{i^*}^d$;
10: Set $\mathcal{Q}[i^*] \leftarrow (\text{destination}(r), \text{true}, t + \text{duration}(p_r))$;
11: End For
12: Update time: $t = t + 1$;
13: End While
Output The multiset of trajectories $\{\tau_i^d\}_{i=1}^{N_b}$.

Algorithm 3 Generation of monthly trajectories

Input Daily trajectory sets $\{\mathcal{T}_d | \forall d \in \mathcal{D}\}$, rebalancing scheme $\{x_{i,j,d} | \forall i, j \in \mathcal{S}, \forall d \in \mathcal{D}\}$, initial inventory $\{z_{s,d} | \forall s \in \mathcal{S}, \forall d \in \mathcal{D}\}$;
1: Initialize vehicle counter $k \leftarrow 0$;
2: For each stand $s \in \mathcal{S}$:
3: For $j = 1$ to $z_{s,1}$:
4: Sample τ uniformly at random from: $\{m \in \mathcal{T}_1 \mid \text{origin}(m) = s\} \cup \{m \in \mathcal{T}_1 | m = \emptyset\}$, where $\emptyset$ denotes an empty route (assignable to any origin);
5: Assign τ to vehicle k and remove τ;
6: Set $\text{station}(k) \leftarrow s$ and record $\text{terminus}(\tau)$ as vehicle k's end-of-day-1 location;
7: Update $k \leftarrow k + 1$;
8: End For
9: End For
10: For $d \in \{1, \dots, |\mathcal{D}| - 1\}$:
11: Relocate $x_{i,j,d}$ bikes from i to j (uniformly at random) $\forall i, j \in \mathcal{S}$;
12: Allocate trajectories for day $d + 1$ to bikes using $z_{s,d+1}$ and a method analogous to Steps 2–8;
13: End For
Output Monthly trajectories $\{\mathcal{T}_l | \forall l \in \mathcal{I}\}$.

reward $\xi(\cdot)$ for road segment e within time period ω is given by:

$$\xi(N_{e,\omega}) = \begin{cases} 1 & \text{if } N_{e,\omega} \ge 1 \\ 0 & \text{if } N_{e,\omega} < 1 \end{cases} \tag{3.11}$$

This binary sampling method tracks whether each spatial–temporal road segment meets the monitoring requirements of the application. By aggregating $N_{e,\omega}$ over all road segments and monitoring periods, the overall sensing reward of the system is quantified as:

$$\Phi = \frac{\sum_{e \in \mathcal{A}} \sum_{\omega \in C} l_e \xi(N_{e,\omega})}{N_C \sum_{e \in \mathcal{A}} l_e} \times 100\% \tag{3.12}$$

where N_C is the total number of time periods. The numerator represents the total length of road segments meeting the sampling requirements, while the denominator reflects the potential total length if all segments meet the requirements. Therefore, Φ represents the proportion of spatial–temporal road segments covered.

3.4.2. Relationship between the number of bikes at stands and the coverage of road segments

Hypothesis: We hypothesize that shared bike coverage of a road segment originating from a single stand follows a binomial distribution. Specifically, given n_s^b shared bikes operating from stand $s \in \mathcal{S}$, assuming independent movement patterns with similar spatial distributions across the road network, the daily coverage of segment $e \in \mathcal{A}$ by bikes from stand s is binomially distributed: $c_{s,e} \sim B(n_s^b, p_{s,e})$. Here, $p_{s,e}$ represents the daily visitation probability of segment e by a bike from stand s. Consequently, the number of times road segment e is expected to be covered daily by n_s^b shared bikes at stand s is given by the binomial expectation:

$$N_{s,e} \approx p_{s,e} n_s^b \qquad \forall s \in \mathcal{S},\ e \in \mathcal{A} \tag{3.13}$$

Verification: To validate the approximation in (3.13), we utilize bike trajectories generated by Algorithm 2. For each stand, we process all daily bike trajectories originating from the stand over a one-month period. From this dataset, we randomly sample trajectory deployments to simulate coverage patterns. Specifically, we fit the daily coverage of road segments across varying bike fleet sizes, with each configuration undergoing 20 independent simulation runs. Results are averaged across these runs to obtain robust estimates. For a fixed stand s and bike fleet size n_s^b, let $N_{s,e}(\tau)$ denote the daily coverage count of road

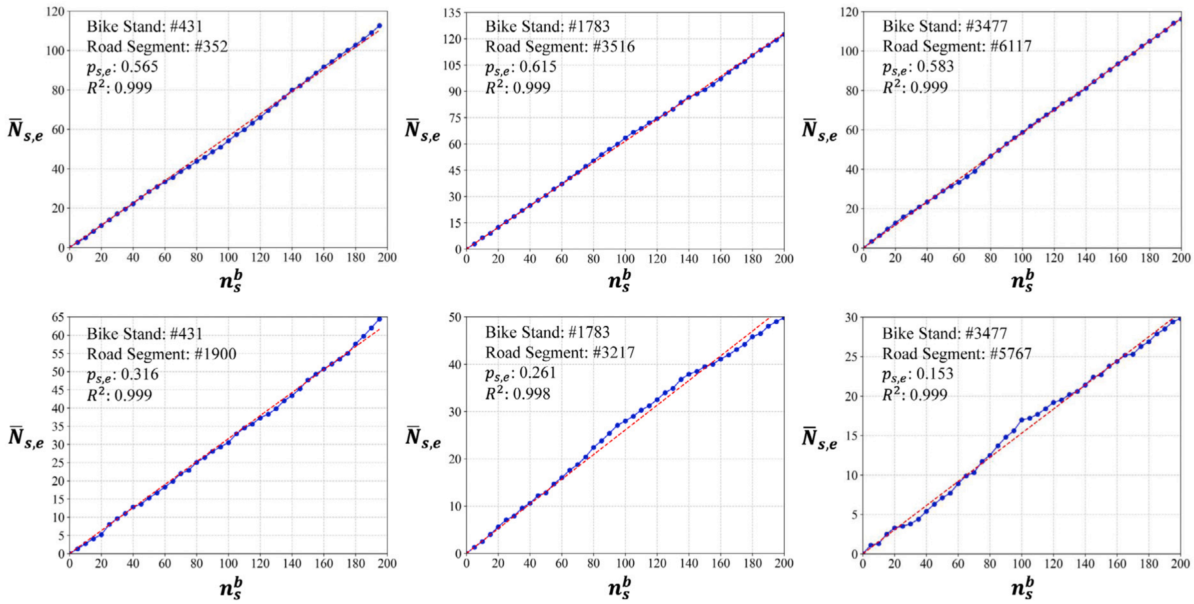

Fig. 7. Empirical relationship between n_s^b and average coverage $\bar{N}_{s,e}$.

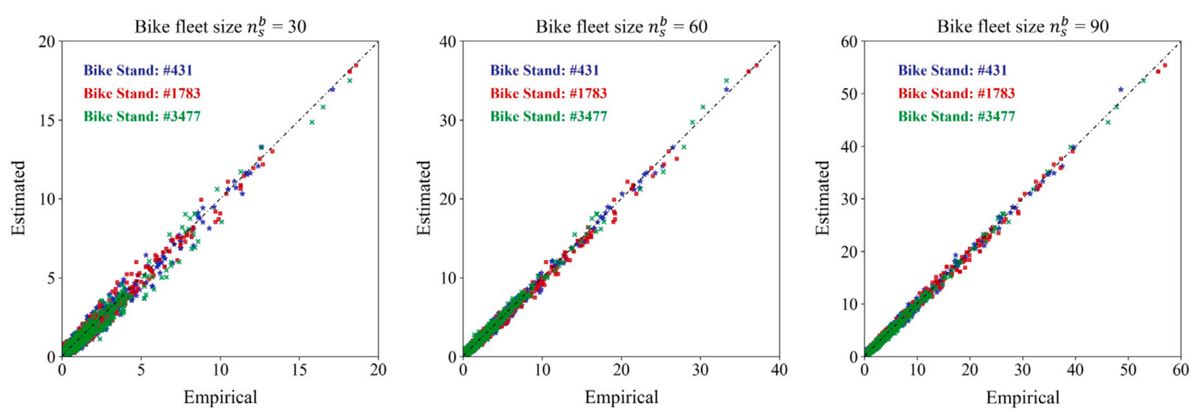

Fig. 8. Scatter plots of empirical vs. estimated coverage for all road segment $e \in \mathcal{A}$.

segment e during the τ-th simulation run ($\tau = 1, \dots, 20$). We define:

$$\bar{N}_{s,e} = \frac{1}{20} \sum_{\tau=1}^{20} N_{s,e}(\tau) \qquad \forall s \in \mathcal{S}, e \in \mathcal{A} \tag{3.14}$$

The empirical relationship between n_s^b and $\bar{N}_{s,e}$ is illustrated in Fig. 7. We observe that for a fixed bike stand s and road segment e, this relationship is approximately linear, consistent with (3.13). Fig. 8 further presents scatter plots comparing estimated versus empirical coverage counts ($N_{s,e}$ vs. $\bar{N}_{s,e}$) for all road segments at three distinct bike fleet sizes: 30, 60, and 90. The strong alignment of data points along the unity line ($y = x$) demonstrates consistent predictive accuracy across operational scales.

Fig. 9 visualizes the visit probability $p_{s,e}$ for bikes from a fixed bike stand to various road segments. The probability is higher for road segments closer to the bike stand, resulting in larger values of the fitting parameter $p_{s,e}$. This pattern reflects the operational characteristics of bike-sharing systems, where bikes tend to circulate more frequently in the vicinity of the bike stand, leading to increased coverage of nearby road segments.

3.4.3. Day-to-day optimization framework for sensor allocation and rebalancing

Given the total number of sensors N_k, the proposed model optimizes sensor allocation and nightly scheduling operations. Solving the model in Section 3.3.2 yields the initial bike inventory $z_{s,d}$ at each stand s at the beginning of day d. This section further determines the initial sensor allocation $x_{s,1}$ to stands on day 1 and the daily dispatch plan $y_{i,j,d}$ for sensor-equipped bikes during subsequent nights. We formulate the sensor allocation and scheduling problem into a rolling-horizon scheme that decomposes the planning horizon into two layers: (i) a static initial allocation for the first day, and (ii) a daily rebalancing procedure for sensor-equipped bikes executed at the end of every day.

Day-1 static allocation model: At day $d = 1$, we determine the initial distribution of the N_k available sensor-equipped bikes across the station network $\mathcal{S}$. The objective is to maximize the sensing reward during the first day. Let $x_{s,1}$ be the number of sensor-equipped bikes at station s of day 1. Binary auxiliary variable $y_e^1 = 1$ if the expected coverage of road segment e exceeds K times. The model of the day-1

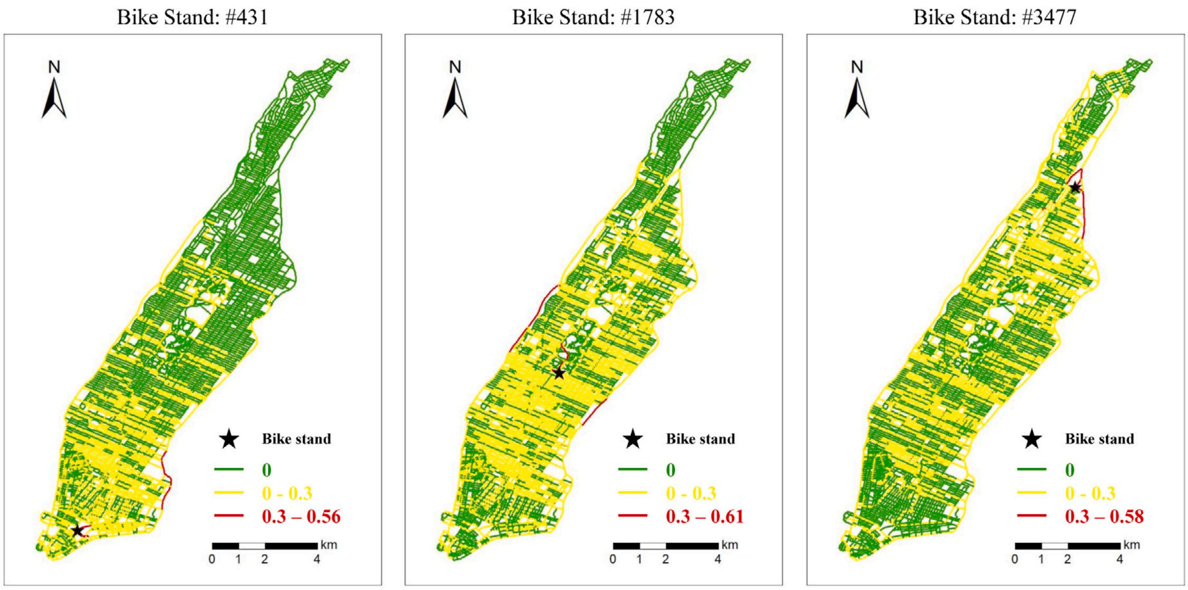

Fig. 9. The visit probability $p_{s,e}$ of each bike from a fixed bike stand to different road segments. The black five-pointed star represents the location of the bike stand, and the heatmap shows the values of the parameter $p_{s,e}$.

sensor allocation problem is as follows:

$$\max \sum_{e\in\mathcal{A}} l_e y_e^1 \tag{3.15}$$

such that

$$N_e^1 = \sum_{s\in\mathcal{S}} p_{s,e} x_{s,1} \ \ \forall e \in \mathcal{A} \tag{3.16}$$

$$-M_1(1-y_e^1) \le N_e^1 - K \ \ \forall e \in \mathcal{A} \tag{3.17}$$

$$N_e^1 - K \le M_1 y_e^1 \ \ \forall e \in \mathcal{A} \tag{3.18}$$

$$\sum_{s\in\mathcal{S}} x_{s,1} = N_k \tag{3.19}$$

$$x_{s,1} \le z_{s,1} \ \ \forall s \in \mathcal{S} \tag{3.20}$$

$$x_{s,1} \in \mathbb{Z}^+ \ \ \forall s \in \mathcal{S} \tag{3.21}$$

$$y_e^1 \in \{0,1\} \ \ \forall e \in \mathcal{A} \tag{3.22}$$

The objective function (3.15) maximizes the total length of road segments where the expected coverage meets the requirement. The expected coverage of road segment e is determined by constraints (3.16). Constraints (3.17)–(3.18) express the binary state of coverage for road segment e, and are equivalent to the following via the big-M method:

$$y_e^1 = \begin{cases} 1 & \text{if} \ \ N_e^1 \ge K \\ 0 & \text{if} \ \ N_e^1 < K \end{cases} \tag{3.23}$$

where M_1 is a sufficiently large number. Constraint (3.19) ensures that the number of allocated sensors does not exceed the total. Constraint (3.20) ensure that the number of sensor-equipped bikes at station s cannot exceed the station's total bike inventory $z_{s,1}$. Constraints (3.21)–(3.22) are the decision variable constraints. The above model can be directly solved by off-the-shelf solvers.

Daily rebalancing model for sensor-equipped bikes: In this section, we address the optimization of the daily rebalancing scheme for sensor-equipped bikes at the end of day d. Given the initial inventory of sensor-equipped bikes $x_{s,d}$ at each station s at the start of day d and the cumulative expected coverage counts α_e for each road segment e within the current time period, we aim to determine the optimal dispatch strategy that maximizes the immediate sensing reward. This optimized reallocation directly yields the updated inventory of sensor-equipped bikes $x_{s,d+1}$ at each station s at the beginning of the next day $d+1$. Let $y_{i,j,d}$ be the number of sensor-equipped bikes dispatched from stand i to stand j at the end of day d. To capture operational dynamics during daytime hours, we introduce $\gamma_{s,d}$ to represent the net change of sensor-equipped bikes at station s due to customer usage on day d. This parameter can be derived from the previous day's result. The daily rebalancing model for sensor-equipped bikes is as follows:

$$\max \sum_{e\in\mathcal{A}} l_e y_e \tag{3.24}$$

such that

$$x_{s,d+1} = x_{s,d} + \gamma_{s,d} + \sum_{i\in\mathcal{S}} y_{i,s,d} - \sum_{j\in\mathcal{S}} y_{s,j,d} \ \ \forall s \in \mathcal{S} \tag{3.25}$$

$$x_{s,d} + \gamma_{s,d} \ge \sum_{j\in\mathcal{S}} y_{s,j,d} \ \ \forall s \in \mathcal{S} \tag{3.26}$$

$$\sum_{s\in\mathcal{S}} x_{s,d+1} = N_k \tag{3.27}$$

$$x_{s,d+1} \le z_{s,d+1} \ \ \forall s \in \mathcal{S} \tag{3.28}$$

$$N_e = \alpha_e + \sum_{s\in\mathcal{S}} p_{s,e} x_{s,d+1} \ \ \forall e \in \mathcal{A} \tag{3.29}$$

$$-M_2(1-y_e) \le N_e - K \ \ \forall e \in \mathcal{A} \tag{3.30}$$

$$N_e - K \le M_2 y_e \ \ \forall e \in \mathcal{A} \tag{3.31}$$

$$x_{s,d+1} \in \mathbb{Z}^+ \ \ \forall s \in \mathcal{S} \tag{3.32}$$

$$y_{i,j,d} \in \mathbb{Z}^+ \ \ \forall i,j \in \mathcal{S} \tag{3.33}$$

$$y_e \in \{0,1\} \ \ \forall e \in \mathcal{A} \tag{3.34}$$

The objective function (3.24) maximizes the total length of road segments where the cumulative expected coverage meets the requirement in the current time period. Constraints (3.25) establishes a deterministic state transition equation that governs the temporal evolution of sensor-equipped bike inventory across the stand network. Constraint (3.26) makes sure that cannot move out more sensor-equipped bikes than actually exist at a stand. Constraints (3.27) ensure that the number of

Algorithm 4 Generating monthly sensor-equipped bike trajectories

Input	Planning horizon $d \in \mathcal{D}$, monitoring period $\omega \in \mathcal{C}$, $P(d) = \omega$ indicates day d belongs to time period ω, daily trajectory sets $\{\mathcal{T}_d \mid \forall d \in \mathcal{D}\}$;
Initialize	Day 1 sensor allocation $x_{s,1}$ via static allocation model Eqs. (3.15)–(3.22), last day's time period: $\omega^* \leftarrow P(1)$, trajectory set of sensor-equipped bikes $\{\mathcal{T}_d^* \mid \forall d \in \mathcal{D}\} = \emptyset$;
1:	For day $d \in \mathcal{D}$:
2:	Determine the time period to day d belongs: $\omega \leftarrow P(d)$;
3:	If $\omega \neq \omega^*$:
4:	Set the cumulative expected coverage counts $\alpha_e = 0$;
5:	Else:
6:	Calculate the cumulative expected coverage counts α_e within the current time period;
7:	Randomly sample sensor-equipped bike trajectories $\mathcal{T}_d^*$ from $\mathcal{T}_d$ based on day d's sensor allocation results;
8:	Calculate $\gamma_{s,d}$ based on the sensor-equipped bike trajectories $\mathcal{T}_d^*$;
9:	Solve daily rebalancing model of day d Eqs. (3.24)–(3.34);
10:	Update $\omega^* \leftarrow \omega$;
11:	Update sensor-based bike positions;
Output	Monthly sensor-equipped bike trajectories $\{\mathcal{T}_d^* \mid \forall d \in \mathcal{D}\}$.

sensor-equipped bikes remains equal to the total N_k. Constraints (3.28) ensure that the number of sensor-equipped bikes at each stand cannot exceed the total number of bikes at that stand. The cumulative expected coverage of road segment e during this time period is determined by constraints (3.29). Constraints (3.30)–(3.31) express the binary state of y_e, where M_2 is a sufficiently large number. Constraints (3.32)–(3.34) are the decision variable constraints. In this study, we set $K = 1$. The above model can be directly solved by off-the-shelf solvers.

Generating monthly sensor-equipped bike trajectories: Building upon the Day-1 static sensor allocation and the daily rebalancing model, we propose an algorithm to construct a complete dispatch strategy for sensor-equipped bikes that generates a monthly bike trajectories while accounting for varying monitoring frequencies. The day-to-day procedure is summarized in Algorithm 4.

4. Results and discussion

All the computational performances reported below are based on a Microsoft Windows 10 platform with Intel Core i9 - 3.60 GHz and 16 GB RAM, using Python 3.12 and Gurobi 9.1.2.

4.1. Evaluation of the optimization strategies

In this section, we evaluate the effectiveness of sensor deployment and dispatch strategies (Section 3.4) for enhancing the sensing power of the bike-sharing system. The two methods compared are as follows:

- **Random sensor allocation and dispatch (Random):** Sensors are randomly assigned to bike stands on the first day. Subsequently, daily bike rebalancing follows the minimum total relocation costs optimization strategy (Section 3.3.2), reflecting standard operational practice.
- **Optimized sensor allocation and dispatch (Optimized):** Both sensor deployment and daily bike rebalancing dispatch are co-optimized using the method in Section 3.4.3 with the objective of maximizing sensing reward.

We plot the sensing reward Φ obtained from the two aforementioned methods across sensor deployments ranging from 100 to 1000. The results, presented in Fig. 10, compare three distinct monitoring frequencies: daily, weekly, and monthly monitoring periods. The findings indicate that: The optimization framework yields a stable 5%–6% gain in sensing reward for daily monitoring frequency. At reduced monitoring frequencies (weekly or monthly), the optimization strategy demonstrates significantly enhanced sensing gains when sensor deployment is sparse (e.g., 100 sensors). Specifically, we observe reward improvements of 8.23% for weekly monitoring and 4% for monthly monitoring. This phenomenon stems primarily from the day-to-day optimization mechanism: sensors can be strategically relocated to new stands at the end of each day, systematically covering previously unmonitored road segments to maximize resource utilization. Fig. 11 visually contrasts road coverage under daily versus weekly monitoring regimes over three consecutive days, using the same 100 sensor-equipped bikes. The weekly regime reveals distinctly complementary coverage distributions across days through day-to-day sensor relocation between monitoring periods. This strategic redeployment delivers substantial sensing reward gains at low sensor counts. However, as deployment scales upward, these gains progressively diminish due to sensing saturation.

4.2. Sensing power of bike-sharing system

In this section, we evaluate the sensing power of the bike-sharing system. The trip data used in the subsequent analysis are from Manhattan, covering 6:00 AM–8:00 PM daily in March 2024. This data has been processed using the methods outlined in Section 3.2.2. A total of 9,581 bikes were identified from the trip data. Additionally, the trajectories of sensor-equipped bikes were generated based on the day-to-day optimization framework for sensor allocation and rebalancing detailed in Section 3.4.3.

Fig. 12 presents the sensing reward Φ for different monitoring frequencies (daily, weekly, monthly). The results indicate that:

(1) Bike-sharing systems demonstrate exceptional low-frequency sensing capabilities: at a monthly interval, 100 bikes ($\approx$ 1% of the fleet) cover 81% of road segments; at a weekly interval, the same 100 bikes achieve 72% spatiotemporal coverage; yet at a daily interval, roughly 1000 bikes ($\approx$ 10%) are required to reach the same 72% coverage.
(2) As the number of sensors increases, the marginal gain in sensing reward decreases, indicating diminishing returns. This suggests that beyond a certain point, adding more sensors provides limited additional benefits. For monthly monitoring, 100 sensors achieve near-optimal coverage, with expansion to 1,000 sensors providing

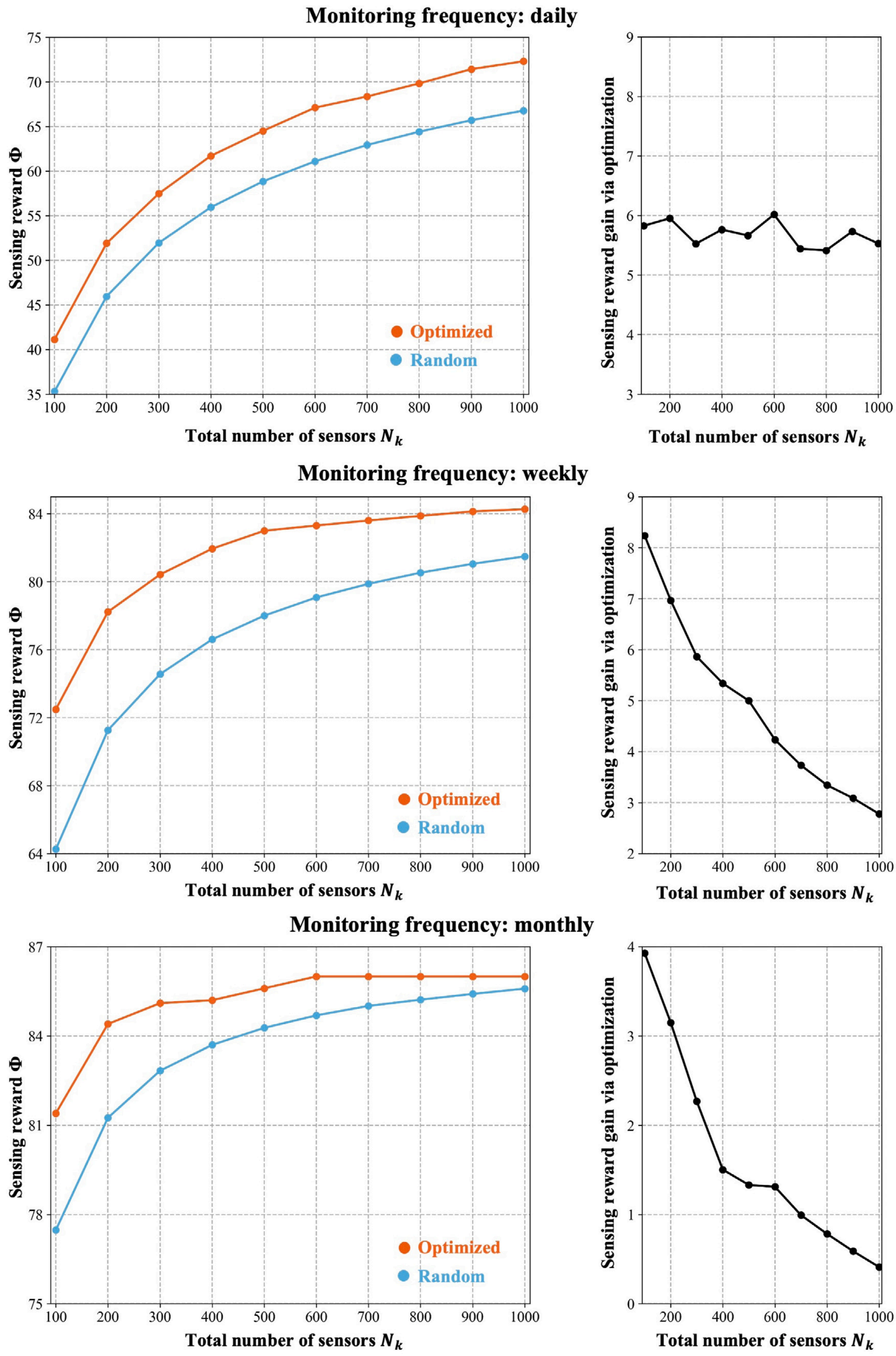

Fig. 10. Left column: Sensing reward Φ for two methods across various total number of sensors N_k; Right column: Sensing reward gain of the optimization method over random method.

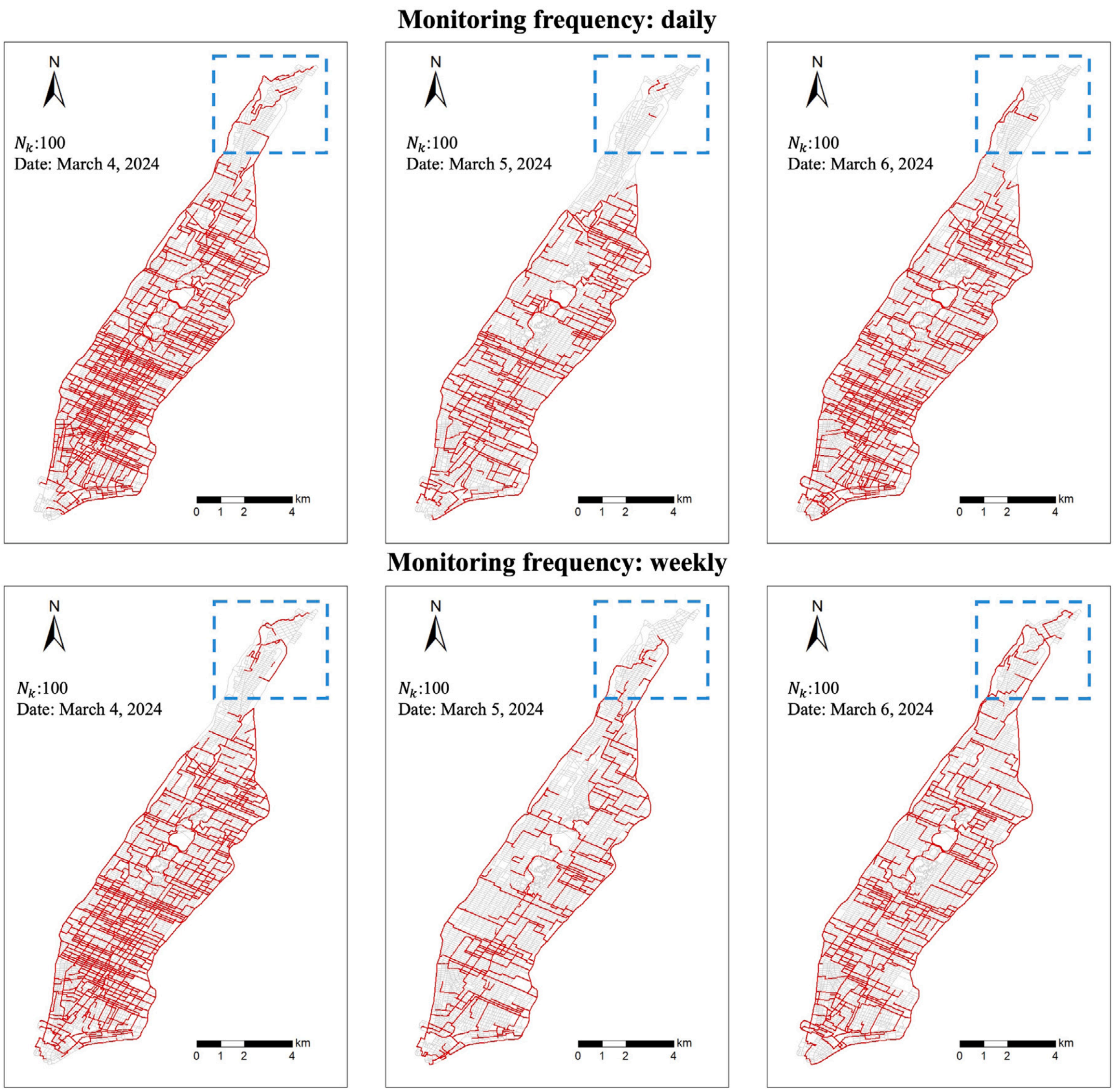

Fig. 11. Visualization of road coverage over three consecutive days under daily versus weekly monitoring frequencies. First line: daily frequency; Second line: weekly frequency. Red segments indicate roads covered by the sensor-equipped bikes.

< 5% total reward improvement. For weekly monitoring, the system approaches saturation at 300 sensors, with subsequent deployment yielding rapidly declining benefits.

Next, we created heatmaps to illustrate the coverage of road segments by 500 sensor-equipped bikes during various days, as shown in Fig. 13. The spatial coverage analysis reveals distinct regional disparities in road segment monitoring, with southern areas exhibiting consistently higher coverage rates compared to northern regions. The heatmap visualization demonstrates stable patterns across observation days, showing persistent coverage in high-activity zones while certain segments remain consistently unmonitored. To address the road segments that are rarely scanned, we can implement fixed monitoring stations or deploy dedicated sensing fleets. These strategies would ensure that underrepresented areas receive the necessary attention for data collection, enhancing the overall sensing capability of the system. By strategically placing fixed monitoring stations in key locations and utilizing dedicated sensing vehicles to target these less frequented segments, we can fill in coverage gaps and improve the comprehensiveness of the spatial data gathered by the bike-sharing system.

4.3. Transferability study

To further understand the sensing power of shared bike fleet beyond the context of a fixed network configuration, we consider two more real-world networks (Fig. 14): The cities of San Francisco and Longquanyi District, Chengdu. The bike-sharing trip data for San Francisco is sourced from Bay Wheels[5] in March 2024, while the data for Longquanyi District comes from Mobike[6] in March 2021. Table 3 summarizes the basic attributes of these three networks, including the number of nodes, edges, stands, daily trips, and bike fleet size.

Transferring the Manhattan experiment to other cities reveals significant differences in sensing reward achieved with identical sensor numbers across networks. For instance, with 100 sensors at monthly monitoring frequency, Manhattan and Longquanyi District achieve approximately 70% to 80% road segment coverage, while San Francisco only reaches 50%. This variation primarily stems from differences in

[5] Bay Wheels: https://www.lyft.com/bikes/bay-wheels/system-data.
[6] This data is not open source.

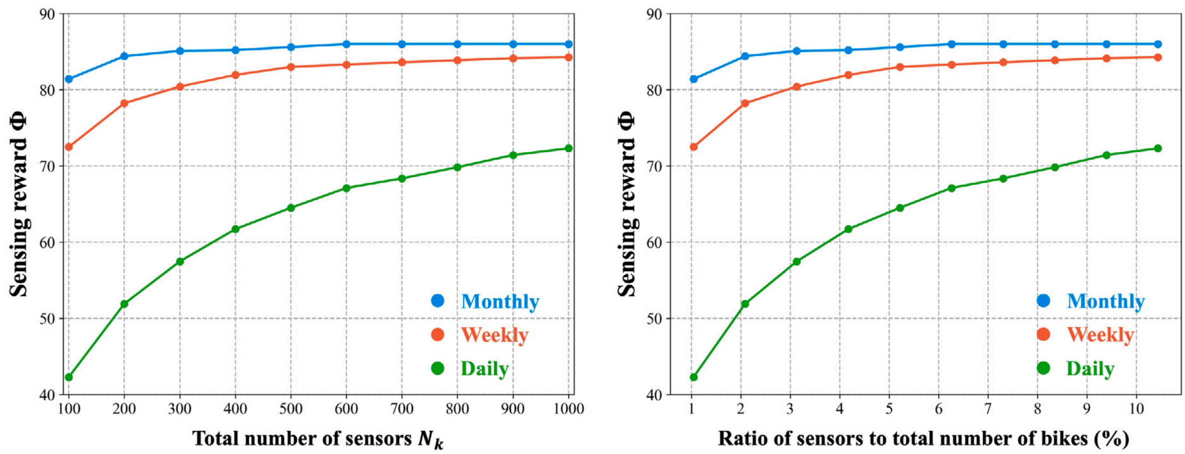

Fig. 12. Sensing reward Φ for different monitoring frequencies: (Left) total number of sensors N_k; (Right) ratio of sensors to total number of bikes.

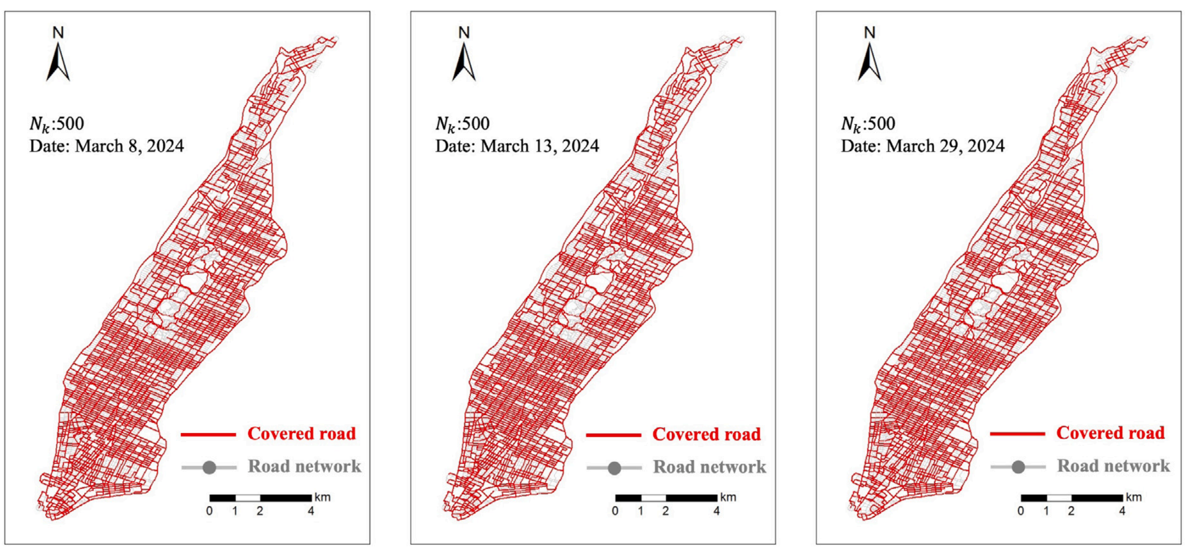

Fig. 13. Visualization of road segment coverage by 500 sensor-equipped bikes over various days (Red segments indicate roads covered by the sensor-equipped bikes).

Table 3
Basic attributes of three bike-sharing networks.

City	Nodes	Edges	Stands	Daily trips	Bike fleet
Manhattan	3,787	6,833	647	6,066–63,379	9,581
San Francisco	7,295	12,392	343	2,207–7,029	2,665
Longquanyi District	1,279	2,081	275	6,529–13,222	1,628

bike usage patterns across regions, where spatial coverage and station distribution remain fundamentally consistent.

5. Conclusion

This study systematically explores the potential of bike-sharing systems as a cost-effective platform for community-level urban diagnostics by simulating sensor deployment and dispatch strategies. The key findings from this study are as follows:

(1) The sensor allocation and dispatch strategy could improve sensing reward by 4%–8% over random deployment in Manhattan.
(2) At a monthly monitoring frequency, only 100 bikes (≈ 1 % of the fleet) could cover 81% of road segments in Manhattan. At a weekly monitoring frequency, same 100 bikes could reach 72% coverage.
(3) As the number of sensors increases, the marginal gain in sensing reward decreases, indicating that sensor deployment strategies should carefully consider the trade-off between coverage and resource allocation.
(4) Persistent hotspots in southern Manhattan contrast with chronically under-scanned northern areas.
(5) Daily coverage patterns are stable, suggesting predictable gaps that fixed stations or dedicated vehicles could fill.

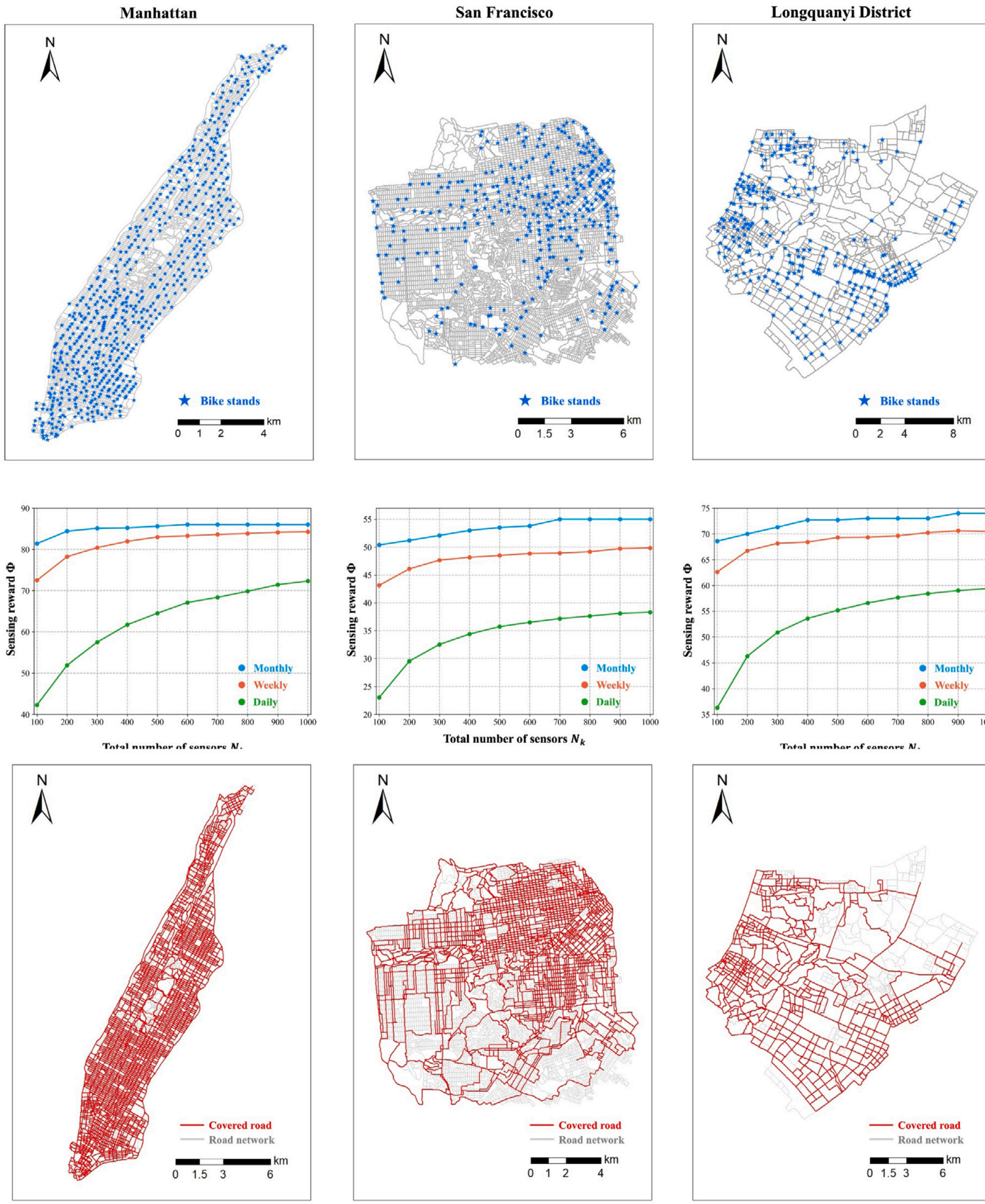

Fig. 14. First row: The three study areas. Second row: Sensing reward Φ versus the number of sensors N_k under different monitoring frequencies. Third row: Visualization of road segment coverage by 100 sensor-equipped bikes over one month.

(6) Transferability studies in San Francisco and Longquanyi District, Chengdu, indicate that sensing power would be governed primarily by local cycling patterns.

By conceptually bridging the gap between bike-sharing operations and urban sensing, this work offers theoretical evidence that shared-bike fleets could serve as low-cost, scalable sensing networks. Nevertheless, the observed cross-city variability underscores the need for pilot field deployments to validate these projections under real traffic, weather, and user-compliance conditions.

Future research should therefore prioritize:

(1) Empirical pilot studies in each city to compare simulated versus actual coverage;
(2) Real-time, adaptive scheduling algorithms that respond to dynamic demand;
(3) Multi-platform integration (e.g., bikes + buses + taxis) to further enhance spatial–temporal sensing power.

CRediT authorship contribution statement

Wen Ji: Writing – original draft, Visualization, Validation, Methodology, Investigation, Formal analysis, Data curation, Conceptualization. **Ke Han:** Writing – review & editing, Supervision, Resources, Methodology, Conceptualization. **Qi Hao:** Writing – review & editing, Visualization, Methodology, Investigation. **Qian Ge:** Writing – review & editing, Methodology, Funding acquisition, Conceptualization. **Ying Long:** Writing – review & editing, Supervision, Resources, Project administration, Funding acquisition, Conceptualization.

Declaration of competing interest

The authors declare no conflict of interests.

Acknowledgments

This work was supported by the National Natural Science Foundation of China (grant numbers 62394331, 62394335, 52178044, 72071163, 72101215), the Science and Technology Department of Sichuan Province (no. 2024JDDQ0007) and Doctoral Innovation Fund Program of Southwest Jiaotong University (no. CX-2025ZD04). We thank Yehao Xia for his assistance in data processing.

Data availability

Data will be made available on request.

References

Agarwal, D., Iyengar, S., Swaminathan, M., Sharma, E., Raj, A., Hatwar, A., 2020. Modulo: Drive-by sensing at city-scale on the cheap. In: Proceedings of the 3rd ACM SIGCAS Conference on Computing and Sustainable Societies. Ecuador, pp. 187–197.

Anjomshoaa, A., Duarte, F., Rennings, D., Matarazzo, T.J., deSouza, P., Ratti, C., 2018. City scanner: Building and scheduling a mobile sensing platform for smart city services. IEEE Internet Things J. 5 (6), 4567–4579.

Ariss, M., Wang, A., Sabouri, S., Duarte, F., Ratti, C., 2024. Drive-by environmental sensing strategy to reach optimal and continuous spatio-temporal coverage using local transit network. Transp. Res. Rec..

Asprone, D., Martino, S.Di., Festa, P., Starace, L.L.L., 2021. Vehicular crowd-sensing: a parametric routing algorithm to increase spatio-temporal road network coverage. Int. J. Geogr. Inf. Sci. 35 (9), 1876–1904.

Birenboim, A., Helbich, M., Kwan, M.-P., 2021. Advances in portable sensing for urban environments: Understanding cities from a mobility perspective. Computers. Environ. Urban Syst. 88, 101650.

Chen, X., Xu, S., Han, J., Fu, H., Pi, X., Joe-Wong, C., Li, Y., Zhang, L., Noh, H.Y., Zhang, P., 2020. PAS: Prediction-based actuation system for city-scale ridesharing vehicular mobile crowdsensing. IEEE Internet Things J. 7 (5), 3719–3734.

Dai, Z., Han, K., 2023. Exploring the drive-by sensing power of bus fleet through active scheduling. Transp. Res. Part E: Logist. Transp. Rev. 171, 103029.

Du, R., Santi, P., Xiao, M., Vasilakos, A.V., Fischione, C., 2019. The sensable city: A survey on the deployment and management for smart city monitoring. IEEE Commun. Surv. Tutor. 21 (2), 1533–1560.

Fekih, M.A., Bechkit, W., Rivano, H., Dahan, M., Renard, F., Alonso, L., Pineau, F., 2021. Participatory air quality and urban heat islands monitoring system. IEEE Trans. Instrum. Meas. 70, 1–14.

Gadsby, A., Watkins, K., 2020. Instrumented bikes and their use in studies on transportation behaviour, safety, and maintenance. Transp. Rev. 40 (6), 774–795.

Gao, Y., Dong, W., Guo, K., Liu Xue Chen, Y., Liu Xiaojin Bu, J., Chen, C., 2016. Mosaic: A low-cost mobile sensing system for urban air quality monitoring. In: IEEE INFOCOM 2016 - the 35th Annual IEEE International Conference on Computer Communications. San Francisco, CA, USA, pp. 1–9.

Glock, K., Meyer, A., 2020. Mission planning for emergency rapid mapping with drones. Transp. Sci. 54, 534–560.

Grubesic, T.H., Wallace, D., Chamberlain, A.W., Nelson, J.R., 2018. Using unmanned aerial systems (UAS) for remotely sensing physical disorder in neighborhoods. Landsc. Urban Plan. 169, 148–159.

Guo, S., Qian, X., 2024. Optimal drive-by sensing in urban road networks with large-scale ridesourcing vehicles. IEEE Trans. Intell. Transp. Syst. 1–12.

Han, K., Ji, W., Nie, Y., Li, Z., Liu, S., 2024. Exploring the sensing power of mixed vehicle fleets. Transp. Res. Part B: Methodol. 190, 103066.

Hasenfratz, D., Saukh, O., Walser, C., Hueglin, C., Fierz, M., Arn, T., Beutel, J., Thiele, L., 2015. Deriving high-resolution urban air pollution maps using mobile sensor nodes. Pervasive Mob. Comput. 16, 268–285.

Hou, Y., Chen, X., Dong, Q., Zhang, F., Sun, Y., Wu, L., Liu, Y., 2025a. Enhancing drive-by sensing power in urban hotspots through multi-objective vehicle selection optimization. Int. J. Geogr. Inf. Sci. 129.

Hou, Y., Chen, X., Huang, Z., Peng, X., Liu, Y., 2025b. Advancing population-targeted urban sensing: A comparative study on mobile and static sensing paradigms. Computers. Environ. Urban Syst. 119, 102288.

Huang, M., Li, X., Yang, M., Kuai, X., 2024. Intelligent coverage and cost-effective monitoring: Bus-based mobile sensing for city air quality. Comput. Environ. Urban Syst. 108, 102073.

Ji, W., Han, K., Ge, Q., 2025. Route planning of mobile sensing fleets for repeatable environmental monitoring tasks. Comput. Environ. Urban Syst. 119, 102285.

Ji, W., Han, K., Liu, T., 2023a. A survey of urban drive-by sensing: An optimization perspective. Sustain. Cities Soc. 99, 104874.

Ji, W., Han, K., Liu, T., 2023b. Trip-based mobile sensor deployment for drive-by sensing with bus fleets. Transp. Res. Part C: Emerg. Technol. 157, 104404.

Kaivonen, S., Ngai, E.C.-H., 2020. Real-time air pollution monitoring with sensors on city bus. Digit. Commun. Networks 6 (1), 23–30.

Li, X., Huo, D., Goldberg, D.W., Chu, T., Yin, Z., Hammond, T., 2019. Embracing crowdsensing: An enhanced mobile sensing solution for road anomaly detection. ISPRS Int. J. Geo-Information 8 (9), 412.

Li, Y., Long, Y., 2024. Inferring storefront vacancy using mobile sensing images and computer vision approaches. Comput. Environ. Urban Syst. 108, 102071.

Li, Y., Meng, X., Zhao, H., Li, W., Long, Y., 2023. Identifying abandoned buildings in shrinking cities with mobile sensing images. Urban Informatics 2 (1), 3.

Ma, Y., Li, Y., Long, Y., 2025. Measuring temporal evolution of nationwide urban physical disorder: An approach combining time-series street view imagery with deep learning. Ann. Am. Assoc. Geogr. 115 (4), 923–948.

Ma, H., Zhao, D., Yuan, P., 2014. Opportunities in mobile crowd sensing. IEEE Commun. Mag. 52 (8), 29–35.

Meng, D., Han, K., 2023. Optimizing vehicle-passenger matching for online ride-hailing with vehicular crowd-sensing. In: 2023 IEEE 26th International Conference on Intelligent Transportation Systems (ITSC). Presented At the 2023 IEEE 26th International Conference on Intelligent Transportation Systems. ITSC, IEEE, Bilbao, Spain, pp. 3527–3532.

Messier, K.P., Chambliss, S.E., Gani, S., Alvarez, R., Brauer, M., Choi, J.J., Hamburg, S.P., Kerckhoffs, J., LaFranchi, B., Lunden, M.M., Marshall, J.D., Portier, C.J., Roy, A., Szpiro, A.A., Vermeulen, R.C.H., Apte, J.S., 2018. Mapping air pollution with google street view cars: Efficient approaches with mobile monitoring and land use regression. Environ. Sci. Technol. 52 (21), 12563–12572.

Nagendra Shiva, S.M., Yasa, P.R., Narayana, M.V., Khadirnaikar, S., Rani, P., 2019. Mobile monitoring of air pollution using low cost sensors to visualize spatio-temporal variation of pollutants at urban hotspots. Sustain. Cities Soc. 44, 520–535.

O'Keeffe, K.P., Anjomshoaa, A., Strogatz, S.H., Santi, P., Ratti, C., 2019. Quantifying the sensing power of vehicle fleets. Proc. Natl. Acad. Sci. 116 (26), 12752–12757.

Shen, S., Zhu, H.Lv.C., Sun, L., Wang, R., 2022. Potentials and prospects of bicycle sharing system in smart cities: A review. IEEE Sensors J. 22, 7519–7533.

Voinea, S.C., Bujari, A., Palazzi, C.E., 2020. Air quality control through bike sharing fleets. In: 2020 IEEE Symposium on Computers and Communications (ISCC). Presented At the 2020 IEEE Symposium on Computers and Communications. ISCC, IEEE, Rennes, France, pp. 1–4.

Wallace, D., Schalliol, D., 2015. Testing the temporal nature of social disorder through abandoned buildings and interstitial spaces. Soc. Sci. Res. 54, 177–194.

Wu, Y., Liu, T., Bo, Du, 2024. Fleet sizing and static rebalancing strategies for shared E-scooters: A case study in Indianapolis. USA, Transp. Res. Part A: Policy Pr. 190, 104287.

Wu, D., Xiao, T., Liao, X., Luo, J., Wu, C., Zhang, S., Li, Y., Guo, Y., 2020. When sharing economy meets IoT: Towards fine-grained urban air quality monitoring through mobile crowdsensing on bike-share system. Proc. ACM Interact. Mob. Wearable Ubiquitous Technol 4, 1–26.

Zhang, X., Yang, Z., Liu, Y., 2018. Vehicle-based bi-objective crowdsourcing. IEEE Trans. Intell. Transp. Syst. 19 (10), 3420–3428.

Zhao, D., Ma, H., Liu, L., 2014. Energy-efficient opportunistic coverage for people-centric urban sensing. Wirel. Netw. 20 (6), 1461–1476.